Available online at www.sciencedirect.com

SciVerse ScienceDirect

Ceramics International 39 (2013) 8025–8034

CERAMICS INTERNATIONAL

www.elsevier.com/locate/ceramint

Structural and electrical properties of $LaNiO_3$ thin films grown on (1 0 0) and (0 0 1) oriented $SrLaAlO_4$ substrates by chemical solution deposition method

D.S.L. Pontes[a], F.M Pontes[b,*], Marcelo A. Pereira-da-Silva[c,d], O.M. Berengue[e], A.J. Chiquito[e], E. Longo[a,f]

[a]*LIEC—Department of Chemistry, Universidade Federal de São Carlos, Via Washington Luiz, Km 235, PO Box 676, 13565-905 São Carlos, São Paulo, Brazil*

[b]*Department of Chemistry, Universidade Estadual Paulista—Unesp, PO Box 473, 17033-360 Bauru, São Paulo, Brazil*

[c]*Institute of Physics of São Carlos, USP, São Carlos 13560-250, São Paulo, Brazil*

[d]*UNICEP, São Carlos 13563-470, São Paulo, Brazil*

[e]*NanO LaB—Department of Physics, Universidade Federal de São Carlos, Via Washington Luiz, Km 235, PO Box 676, 13565-905 São Carlos, São Paulo, Brazil*

[f]*Institute of Chemistry, Universidade Estadual Paulista—Unesp, Araraquara, São Paulo, Brazil*

Received 26 February 2013; received in revised form 18 March 2013; accepted 20 March 2013
Available online 29 March 2013

Abstract

$LaNiO_3$ thin films were deposited on $SrLaAlO_4$ (1 0 0) and $SrLaAlO_4$ (0 0 1) single crystal substrates by a chemical solution deposition method and heat-treated in oxygen atmosphere at 700 °C in tube oven. Structural, morphological, and electrical properties of the $LaNiO_3$ thin films were characterized by X-ray diffraction (XRD), atomic force microscopy (AFM), field emission scanning electron microscopy (FE-SEM), and electrical resistivity as temperature function (Hall measurements). The X-ray diffraction data indicated good crystallinity and a structural preferential orientation. The $LaNiO_3$ thin films have a very flat surface and no droplet was found on their surfaces. Samples of $LaNiO_3$ grown onto (1 0 0) and (0 0 1) oriented $SrLaAlO_4$ single crystal substrates reveled average grain size by AFM approximately 15–30 nm and 20–35 nm, respectively. Transport characteristics observed were clearly dependent upon the substrate orientation which exhibited a metal-to-insulator transition. The underlying mechanism is a result of competition between the mobility edge and the Fermi energy through the occupation of electron states which in turn is controlled by the disorder level induced by different growth surfaces.

Keywords: Chemical solution deposition; Thin films; $LaNiO_3$; $SrLaAlO_4$

1. Introduction

Metal-to-insulator transitions (MIT) has been studied in a large variety of systems. These transitions are normally driven by typical parameters such as doping, pressure, temperature and dimensionality (thickness). Metallic perovskites oxides such as $La_{0.5}Sr_{0.5}CoO_3$ (LSCO) [1], $LaNiO_3$ (LNO) [2,3], LaSrMnO (LSMO) [4], $Ca_{2-x}Sr_xRuO_4$ (CSR) [5] and $SrRuO_3$ (SRO) [6] are examples of excellent candidates to explore basic science regarding MIT. These materials can be characterized as strongly electron correlated interactions due to their metallic behavior which in turn is highly dependent upon the dimensionality of the system. Among these materials, the entire class of rare-earth nickelates $RNiO_3$ is known to display MIT which is usually associated with a variation of the unit cell volume as a function of temperature and the radius of the rare-earth material. Of these materials, rare-earth nickelate $LaNiO_3$ is the most interesting, and, surprisingly, $LaNiO_3$ does not present MIT in its bulk form but instead displays a metallic-like behavior in a wide range of temperatures and even in a few Kelvins range [7,8].

$LaNiO_3$ is also the most technologically relevant conductive metallic oxide because it exhibits a simple pseudocubic

*Corresponding author. Tel.: +55 14 3103 6135; fax: +55 14 3103 6088.
E-mail address: fenelon@fc.unesp.br (F. Pontes).

0272-8842/$ - see front matter © 2013 Elsevier Ltd and Techna Group S.r.l. All rights reserved.
http://dx.doi.org/10.1016/j.ceramint.2013.03.072

perovskite structure with a small degree of rhombohedral distortion as well as a relatively simple composition and stoichiometry which enables easier control of the final product during synthesis. Additionally, the pseudocubic perovskite structure has a lattice parameter very close to many monocrystalline substrates, ferroelectric and multiferroic materials. This property is considerably beneficial to obtain highly texturized or epitaxial $LaNiO_3$ thin films for use in different device architectures such as substrate/$LaNiO_3$, $LaNiO_3$/ferroelectric and $LaNiO_3$/multiferroic. Thus, $LaNiO_3$ also attracted significant attention, especially as a bottom electrode for replacing platinum electrodes in resistance random access memories and ferroelectric or dielectric capacitors when the appreciable metallic conductivity favors integration in electro-electronic devices. Many authors reported that ferroelectric and dielectric properties for thin films such as $PbZr_{1-x}Ti_xO_3$ (PZT) [9,10], $Ba_{1-x}Sr_xTiO_3$ (BST) [11], $PbTiO_3$ [12], $(K,Na)NbO_3$ [13] and $BaTiO_3$ (BT) [14] are significantly improved with the use of a $LaNiO_3$ bottom electrode. In a previous study, we observed that ferroelectric and dielectric properties for highly (1 0 0) oriented $Pb_{0.80}Ba_{0.20}TiO_3/LaNiO_3$ heterostructure grown on a $LaAlO_3$ (1 0 0) substrate by a chemical solution deposition (CSD) method are considerably better when $LaNiO_3$ is used as a bottom electrode [15]. Recent investigations have shown that single crystal substrates with different conductivity, thickness and orientation also play an important role in chemical and physical properties of $LaNiO_3$ thin films. Recent papers have shown that epitaxial ultrathin films of $LaNiO_3$ grown on (0 0 1) $SrTiO_3$ [16], $(LaAlO_3)_{0.3}(SrAlTaO_6)_{0.7}$ [17] and $DyScO_3$ [18] substrates by rf magnetron sputtering display MIT which is dependent on both the thickness and the type of substrate. The authors correlated the phenomenon by a combination of epitaxial strain and a reduction in the dimensionality for electron transport in those thin films.

To the best of our knowledge, several works in literature report a significant understanding on the LNO thin films deposited on different oxide substrates such as $SrTiO_3$ (STO), $LaAlO_3$ (LAO) and MgO [19–21]. However, until now, details concerning the deposition of nanostructured $LaNiO_3$ (LNO) thin films by chemical solution deposition (CSD) method and grown on (1 0 0) and (0 0 1) oriented $SrLaAlO_4$ single crystal substrate have not been investigated systematically. We report herein the growth, structural, microstructural and electrical properties of nanostructured $LaNiO_3$ thin films grown on (1 0 0) and (0 0 1) oriented $SrLaAlO_4$ single crystal substrates by using a chemical solution deposition method. The combined results of X-ray diffraction (XRD), atomic force microscopic (AFM), field emission scanning electron microscopy (FE-SEM), and electrical resistivity as temperature function indicated that the growth LNO thin films on different surfaces introduced an interesting and fruitful way to investigate the role of disorder on MIT in this material. The dependence of the observed conduction mechanisms on sample thickness and crystallographic direction is described within a framework where disorder plays a fundamental role. In fact, the properties of $LaNiO_3$ can be artificially tailored to easily control chemical and physical properties.

2. Experimental procedures

$LaNiO_3$ thin films (therein referred as LNO) were prepared using a chemical solution deposition (CSD) method. The starting chemicals were lanthanum nitrate $[La(NO_3)_3]$ and nickel acetate $[Ni(CH_3COOH)_2 \cdot 4H_2O]$ from Alfa Aeasar Co. Water, citric acid and ethylene glycol were used as solvent, chelanting, and polymerizing agents, respectively. The nickel acetate was dissolved in a water solution of citric acid under constant agitation to produce Ni-Citrate. Then, an equimolar amount of lanthanum nitrate was dissolved in distilled water, held at room temperature, and the two solutions were mixed together under constant stirring. After the homogenization of the solution containing La and Ni cations, ethylene glycol was added to promote the citrate polymerization by the polyesterification reaction. With continued heating at 80–90 °C, the solution became more viscous, albeit devoid or any visible phase separation. The viscosity of the deposition solution was adjusted to 15 mPa/s by controlling the water content. Prior to coating, the $SrLaAlO_4$ substrates was cleaned by immersion in a sulfochromic solution followed by rinsing several times in deionized water. Substrates were then dried in an oven at 100 °C for about one hour.

The polymeric precursor solution was spin-coated on substrates [$SrLaAlO_4$ (1 0 0) and $SrLaAlO_4$ (0 0 1)] by a spinner operating at a range of 5000–9000 rev/min for 30 s using a commercial spinner (spin-coater KW-4B, Chemat Technology). Two-stage heat treatment was carried out as follows: initial heating at 400 °C for 4 h at a heating rate of 5 °C/min in an oxygen atmosphere to pyrolyze the organic materials followed by heating at 700 °C for 2 h at a heating rate of 5 °C/min for crystallization in an oxygen atmosphere. The film thickness was controlled by adjusting the number of coatings and the rotation. Each layer was pyrolyzed at 400 °C and crystallized at 700 °C before the next layer was deposited. These coating/drying operations were repeated until the desired thickness was obtained (50–450 nm).

LNO thin films were then structurally characterized by XRD in the 2θ–θ scan mode (steps of 0.02°) which was recorded on a Rigaku D/Max 2400 diffractometer. The thickness of the thin films was characterized using FE-SEM (FEG-VP Zeiss Supra 35, with a secondary electron detector on a freshly fractured film/substrate cross-section. Atomic force microscopy (AFM) was used to obtain a bi-dimensional image reconstruction of the sample surface. These images provided an accurate analysis of the sample surface and the quantification of parameters such as roughness and grain size. A Digital Instruments Multi-Mode Nanoscope IIIa was used in these experiments.

The devices were patterned into Hall bars prepared by standard lithography and chemical etching (see Fig. 5b). The Ohmic contacts were fabricated by depositing 100 nm of Au. A conventional ac four-probe method was used to measure all the electrical parameters. The transport measurements were carried out at different temperatures from 8 K to 300 K ($\pm$0.1 K) using a closed-cycle helium cryostat and at a pressure lower than 10^{-6} Torr. The resistivity was obtained by using standard low-frequency ac lock-in techniques (f=13 Hz)

with a high noise rejection ratio; dc measurements were also used, but the results remain unchanged. The measurements were taken at both increasing and decreasing temperatures, and no hysteresis was observed in the entire temperature range. Different values for the current used in the experiments were used to avoid nonlinear transport due to high field effects or Joule heating.

3. Results and discussion

Fig. 1 shows X-ray patterns for representative films from three different thicknesses on (1 0 0) and (0 0 1) oriented $SrLaAlO_4$ substrates. The pseudo-cubic lattice parameter of the bulk LNO is 3.840 Å [22]. $SrLaAlO_4$ substrates have tetragonal structure, which is in this system defined as pseudo-cubic symmetries with lattice parameters $a=3.756$ Å [23]. According to bulk LNO pseudo-cubic lattice parameters, the lattice mismatch value is −2.2% compressive strain for (1 0 0) and (0 0 1) oriented $SrLaAlO_4$ substrates. As we known, strain phenomenon and epitaxial or textured growth are strongly dependent of a critical thickness, deposition method, mismatch between thin film and substrate [24–27].

As revealed from the XRD patterns, all peaks indexed in Fig. 1 correspond to perovskite phase, which indicates that the

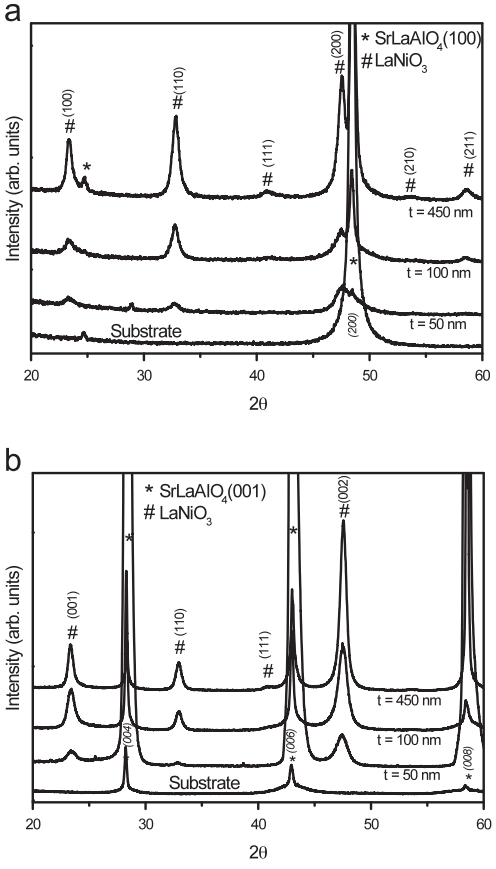

Fig. 1. Structural characterization of $LaNiO_3$ thin films of different thicknesses by X-ray diffraction: (a) X-ray θ–2θ scans showing both the effects of film thickness and orientation on $SrLaAlO_4$ (1 0 0) substrates, and (b) X-ray θ–2θ scans showing both the effects of film thickness and orientation on $SrLaAlO_4$ (0 0 1) substrates. t=thickness.

all LNO thin films possess a pseudo-cubic symmetry well crystallized into single phase, irrespective both (0 0 1) and (1 0 0) $SrLaAlO_4$ substrates. However, preferred oriented or textured LNO thin films demonstrated XRD patterns with certain diffraction reflections more pronounced than the others which was strongly dependent on the orientation of the $SrLaAlO_4$ substrate. Moreover, with increasing thickness, intensities of (1 0 0), (1 1 0) and (2 0 0) diffraction peaks, showed distinct behavior on the two different orientations. Significantly, XRD patterns of LNO thin films grown on (0 0 1) oriented $SrLaALO_4$ substrate exhibits strong (0 0 l) plane family diffractions peaks, suggesting that textured LNO thin films with preferred strong orientation on (0 0 1) oriented $SrLaALO_4$ substrate. In addition, bulk powder and polycrystalline thin films samples indicate that the (1 1 0) diffraction peak should be the most intense, followed by (2 0 0), (1 1 1), and (1 0 0) diffraction peaks, respectively [28]. This is clearly not the case for the current LNO thin films grown on (0 0 1) oriented $SrLaALO_4$ substrate, irrespective of the thickness. Surprisingly, all LNO thin films deposited on (1 0 0) oriented $SrLaAlO_4$ substrate (see Fig. 1a), exhibited almost same intensity (1 1 0) diffractions peak when compared (1 0 0) and (2 0 0) diffraction peaks. According to the relative intensity of the (1 0 0), (1 1 0) and (2 0 0) diffraction peaks, a weak texturing along (h 0 0) direction has been observed, suggesting that the LNO thin films are almost grown in random orientation and/or lightly textured with preferred weaker orientation. These characteristics on the preferred crystallographic directions can lead to anisotropic properties in LNO thin films (to be discussed in the next paragraphs).

In order to analyze texture in the films, the relative ratios of the intensities of the diffraction peaks obtained for a textured sample provide information on the degree orientation, known as *Lotgering factor* [29,30]. This factor is defined for a *hkl* orientation as:

$$F = (P-P_0)/(1-P_0)$$

where F denotes the orientation factor with respect to a reference plane ($h\,k\,l$), the P factors are obtained from the diffraction patterns of the textured thin films (P) and from the patterns of an equivalent sample with random orientation (P_0), and are defined by:

$$P = \Sigma\, I(h\ 0\ 0)/\Sigma\, I(h\ k\ l)$$

being $I(h\,k\,l)$ the intensities of the diffraction peaks. The values of the orientation factor may vary from 0 to 1. An orientation factor 0 indicates random oriented sample and 1 ideally oriented sample. The higher the value obtained, the more oriented the sample for that direction, i.e., implies high texture.

In the present study the orientation factor of the LNO thin films calculated from the X-ray diffraction patterns is shown in Table 1 for (h00) and (00l) direction as a function of film thickness and substrate orientation. The analysis of the orientation factor values indicates important aspects; (i) all films are textured; (ii) the highest F value is observed for the thinnest film and gradually decreases with increasing film thickness; (iii) furthermore, for all LNO thin films grown on

(1 0 0) oriented $SrLaAlO_4$ substrate, *F* values were lower than for same films grown on (0 0 1) oriented $SrLaAlO_4$ substrate, indicating texture weak in (1 0 0) preferred orientation.

As clearly shown in Fig. 1, with increasing thickness, more and more intense is (1 1 0) reflections. This phenomenon should be generated to relieve strain between film/substrate interface, and as the thickness reaches a critical value above 50 nm the strain will be completely relaxed causing a deflection of preferential growth. This characteristic is intrinsic to the chemical solution deposition method where the processing steps involved in forming thick films undergo successive deposition and heat treatment cycles (heating and cooling). In our case, the 50 nm thick films were prepared in a step single deposited directly on (1 0 0) or (0 0 1) oriented $SrLaAlO_4$ substrates resulting in a strain and preferred orientation effects (see orientation factor values, Table 1). In contrary, to obtain 100 nm and 450 nm thick films, successive depositions and heat treatment cycles were realized, as consequence more and more dislocations should occur with strain energy released, suggesting preferred orientation degree small compared with 50 nm thick films. A schematic diagram can be draw to illustrates this, as shown in Fig. 2.

Table 1
Orientation degree (*F*), average crystallite size (*d*), lattice parameters (*a*), and (*t*) average grain size by AFM of LNO thin films on (1 0 0) $SrLaAlO_4$ and (0 0 1) $SrLaAlO_4$ single crystal substrate as function thickness.

Orientation	1 0 0			0 0 1		
Thickness	450 nm	100 nm	50 nm	450 nm	100 nm	50 nm
Parameters						
a (nm)	0.3850	0.3850	0.3849	0.3835	0.3826	0.3821
d (nm)	12.1	9.1	7.5	13.1	9.3	9.1
t (nm)	30	25	15	35	30	20
F	0.50	0.26	0.75	0.84	0.82	0.91

As we known, the preferred orientation mechanism is stronger dependent of the crystallographic planes. Generally, energy minimization considerations and their relation to chemical termination of the substrate surface and film has been exhaustively discussed by many authors in terms of surface energy either from viewpoint theoretical or experimental [31–36]. In this framework, surface energy is one of the central issues to obtain coherent (epitaxial) or strongly textured growth.

Therefore, the changes in the degree of preferred orientation in our case should be related to the different surface energies characteristic of each substrate surface. Certainly, the surface energy is different when the orientation of the substrate is changed of (0 0 1) to (1 0 0). Thus, it is possible that more energy (a higher temperature) is required to obtain highly textured LNO thin films on the (1 0 0) $SrLaAlO_4$ substrate rather than on the (0 0 1) $SrLaAlO_4$ substrate; i.e., the film has a tendency to be highly oriented toward the lowest energy plane. Thus, we propose that the smaller degree of orientation of the LNO film on a (1 0 0) oriented substrate may be due to the higher energy of the (1 0 0) surface rather than the lattice match between LNO and $SrLaAlO_4$ single crystal substrates.

Recently, Antonakos et al. [37] reported $La_{0.5}Ca_{0.5}MnO_3$ films of various thickness grown on (0 0 1) oriented $SrLaAlO_4$ single crystal substrates by pulse laser deposition; The X-ray diffraction measurements showed that films epitaxial grown in (0 0 l) direction. In addition, Pervolaraki et al. [38] reported $La_5Ca_9Cu_{24}O_{41}$ films on (1 0 0) oriented $SrLaAlO_4$ single crystal substrates prepared by pulse laser deposition technique; The films exhibits mainly (0 *k* 0) preferred orientation although peak for polycrystalline samples, remains present. In the other

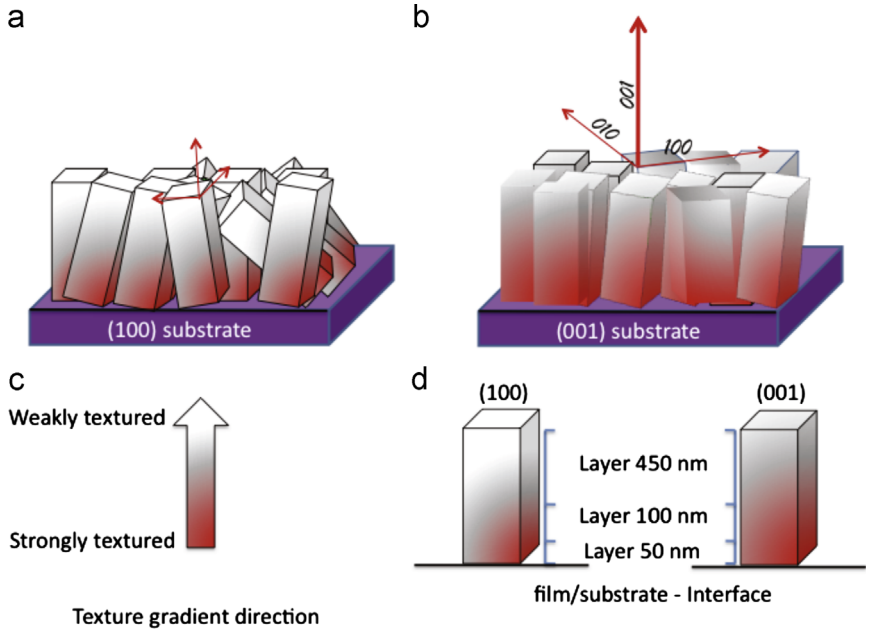

Fig.2. Schematic diagram of the anisotropic texture gradient induced by the substrate's vicinality and film thick. (a) A view of the texture variation on a (1 0 0) surface structure, weakly textured. (b) A view of the texture variation on a (0 0 1) surface structure, strongly textured. (c) The red and white colors correspond to the strongly and weakly textured states, respectively. (d) Thickness gradient direction.

hand, is known that epitaxial LNO thin films tend to exhibit a strong (h 0 0) orientation on $SrTiO_3$ and $LaAlO_3$ crystal single substrates [39,40].

In addition, Fig. 1 shows that when film thicknesses are increased from 50 nm to 450 nm, the intensity of the LNO (0 0 2) and (2 0 0) peaks increases as well, but the full width at half maximum (FWHM) decreases, which indicates that the grain size increased and/or crystallite. In these two cases, we have also estimated the crystallite sizes by using the known Scherrer's equation (see Table 1).

The morphology of LNO thin films was also investigated by AFM, and the results are displayed in Fig. 3. All these samples exhibited a dense and uniform microstructure with spherical-shaped grains. The observed average grain size of the films on (1 0 0) and (0 0 1) $SrLaAlO_4$ substrates increases from 10 nm to 30 nm and 15 nm to 35 nm, respectively, suggesting that the grains are formed of at least two or three crystallite, which is qualitatively consistent with XRD results. In addition, films grown on the (1 0 0) surface have a smaller average grain size than films grown on the (0 0 1) surface. All the thin films have smooth surfaces with root-mean-squared (RMS) roughness below 5 nm. In particular, several groups had investigated the growth mechanism (surface aspects) of LNO thin films on different substrates and using various deposition techniques. $LaNiO_3$ thin films deposited on (1 0 0) $SrTiO_3$ single crystal substrate using a similar procedure described by Mambrini et al. [41] shown elongated grains, with typical length and width values of 150 nm and 60 nm, respectively. Recently, Awan et al. [42] reported $LaNiO_3$ thin films grown on (1 0 0) Si substrates by pulsed laser deposition technique. Atomic force microscopic analysis was employed to characterize surface morphology; the average grain size of the LNO thin films was 200 nm. Liang and Xiaofang [43] investigated the growth mechanism of LNO films on single crystal (1 0 0) silicon substrates fabricated by RF magnetron sputtering method. The authors reported that the LNO film deposited at 400 °C shows an amorphous structure without grains on the surface, while grains with an average size of 8 nm, 25 nm, 36 nm and 43 nm were observed to LNO films deposited at 500 °C, 600 °C, 700 °C and 800 °C, respectively.

As a matter of fact, the orientation of the substrate directly influences the growth rate of the grains and the degree of orientation. Along with the film thicknesses, we believe that these parameters play a key role in electrical properties of LNO thin films which will be explored in this work.

Cross section analysis of these films were performed by FE-SEM (FEG-VP Zeiss Supra 35) and revealed that samples display similar thickness of approximately 50 nm, 100 nm and 450 nm on both (1 0 0) and (0 0 1) $SrLaAlO_4$ single crystal substrates (see Fig. 4).

Fig. 5a is a sketch of the experimental device geometry used for electron transport measurements. In addition, Fig. 5b shown a real view of the samples used in our measurements. Besides the high electrical conductivity, the sample of 50 nm in thickness still remains transparent to visible light. Additionally in detail it can be seen the Hall bar geometry (in brown) defined by combining lithographic and chemical etching techniques used for transport measurements.

The temperature dependent resistivity data obtained for samples of different thicknesses grown on substrates with (1 0 0) and (0 0 1) orientations are shown in Figs. 6 and 7, respectively. Both thickness and substrate orientation induce dramatic changes in the electron transport in these samples. Beginning with the resistivity dependence on the thickness

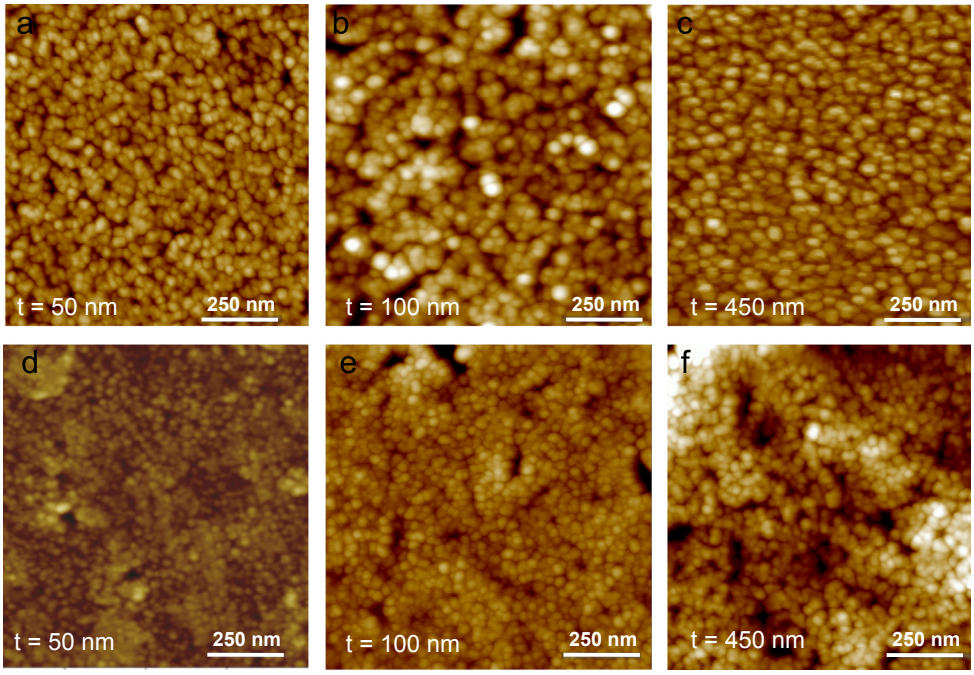

Fig. 3. Top view of $LaNiO_3$ for samples of different thicknesses grown onto $SrLaAlO_4$ substrates with (0 0 1) [a,b,c] and (1 0 0) [d,e,f] orientations which were taken by scanning force microscopy, 1 μm × 1 μm image scan.

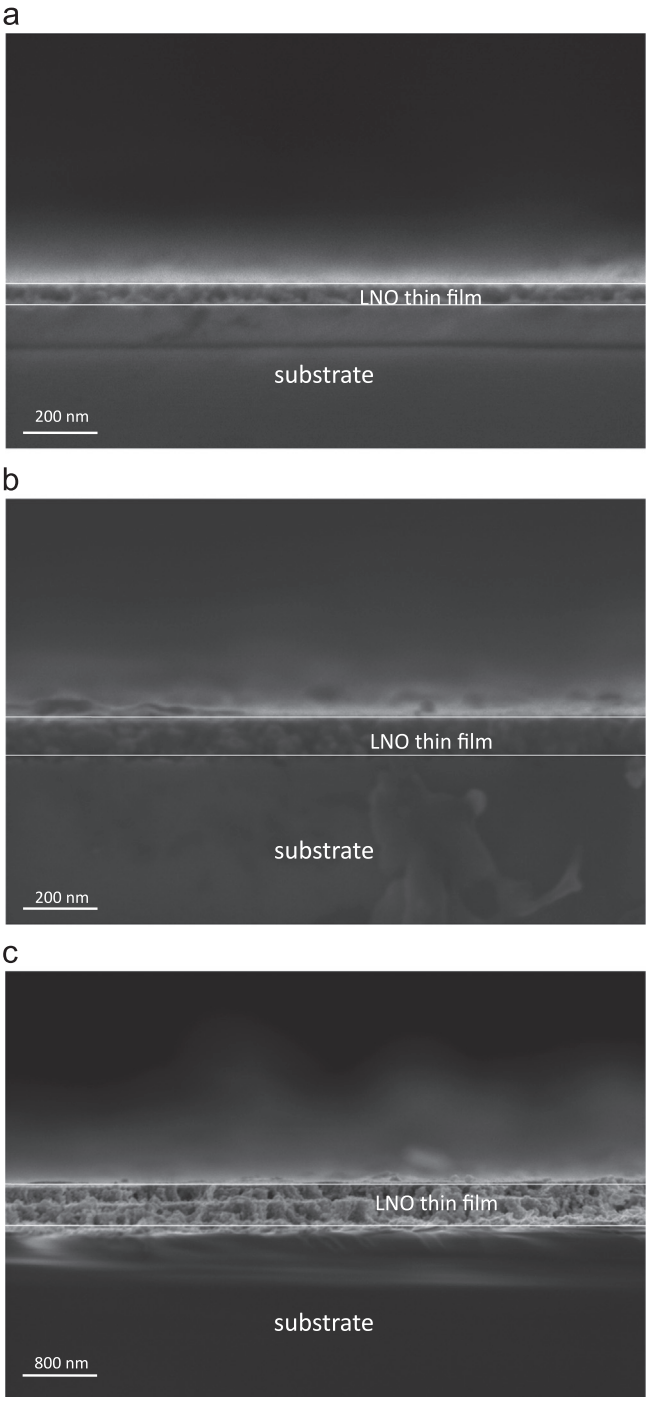

Fig. 4. Cross-sectional FE-SEM micrographs of LNO films with thicknesses of about (a) 50 nm; (b) 100 nm and (c) 450 nm on (1 0 0) $SrLaAlO_4$ substrate.

of the films, samples grown on the (1 0 0) surface exhibit a monotonic activated-like behavior for all film thicknesses such as the behavior observed in insulating or semiconducting materials (see Fig. 6). In addition to the crystalline quality of the samples, the presence of disorder cannot be avoided; as a consequence, the electron potential is also disordered.

Any carrier subjected to a random potential is unable to move freely through the system if either potential fluctuations exceed a critical value or the electron energy is lower than the characteristic value of the potential fluctuations, leading to

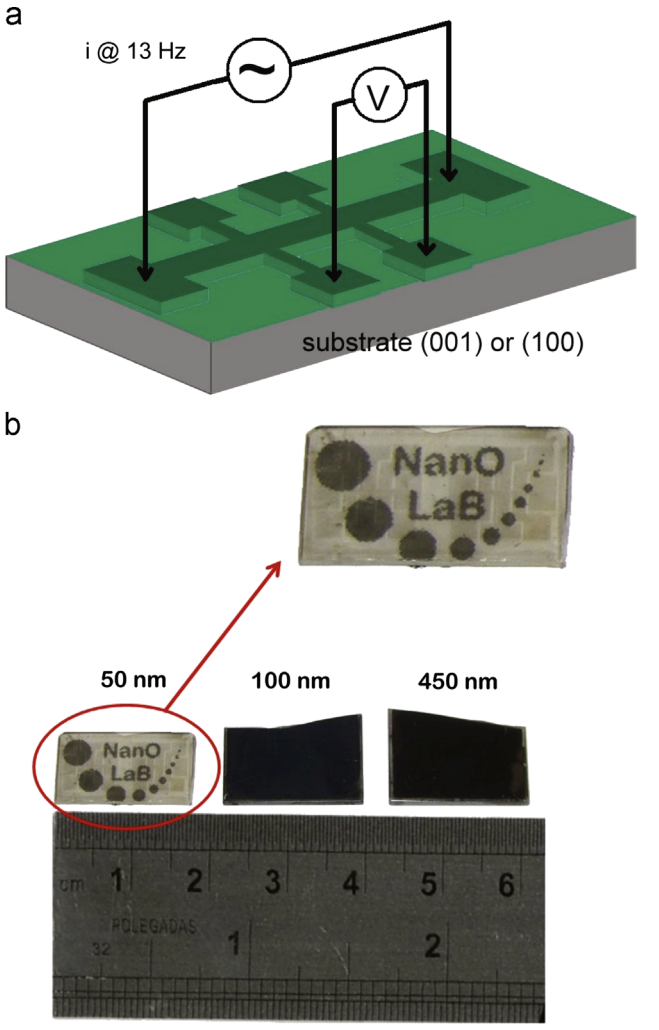

Fig. 5. Experimental devices patterned into Hall bars prepared by standard lithography and chemical etching (a), and a real view of the samples used in our measurements (b). The Hall bar geometry (in brown) is defined by combining lithographic and chemical etching techniques used for transport measurements (in details red arrow). (For interpretation of the references to color in this figure legend, the reader is referred to the web version of this article.)

Anderson-type localization and hence explain the observed insulating behavior [44,45]. Considering the motion of charges in disordered potentials, the expected conduction mechanism (metallic) will change its character to an activated process such as the variable range hopping (VRH) reported by Mott [46], for instance. In this model, phonons are required to conserve energy during a hop from site to site; a higher phonon density at a higher temperature increases the hopping rate and thereby decreases the resistivity. The VRH mechanism is described by the equation [46].

$$\rho(T) = \rho_0 exp\left(\frac{T_0}{T}\right)^{1/4}, \quad (1)$$

where $T_0 = 5.7\alpha^3/k_B N(E_F)$, $N(E_F)$ is the density of states at the Fermi level and α^{-1} is the localization length. The VRH mechanism normally occurs only in the temperature region where the energy is insufficient to excite the charge carrier across the Coulomb gap between two states. Hence conduction

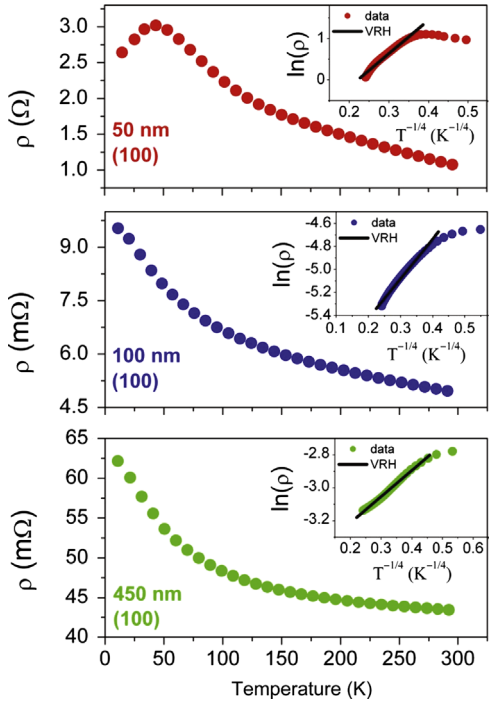

Fig. 6. Temperature dependence of the electrical resistivity of the $LaNiO_3$ samples grown on (1 0 0) $SrLaAlO_4$ single crystal substrate and with different thicknesses: 50 nm, 100 nm and 450 nm. All (100) samples present an insulator behavior.

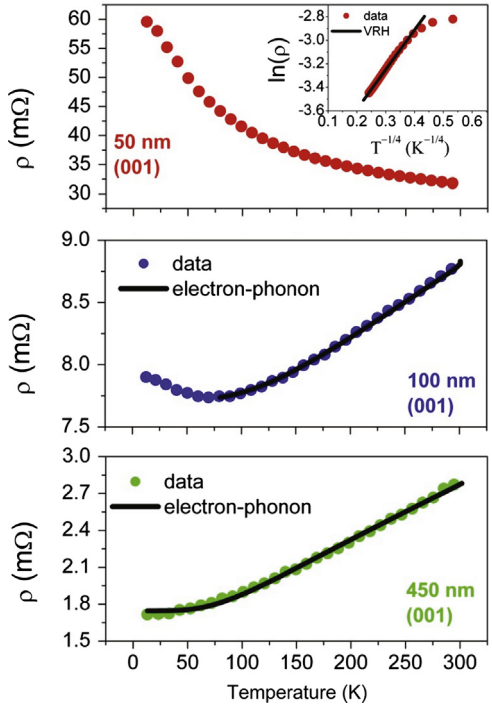

Fig. 7. Temperature dependence of the electrical resistivity of the $LaNiO_3$ samples grown on $SrLaAlO_4$ (0 0 1) single crystal substrate and with different thicknesses: 50 nm, 100 nm and 450 nm; It is evident in the 100 nm thick sample when the insulating behavior is replaced by a metallic behavior which is expected in MIT.

takes place by the hopping of a small region (k_BT) in the vicinity of the Fermi level where the density of states remains almost a constant ($m=1/4$). This condition is fulfilled when the temperature is sufficiently small or when the energy states are uniformly distributed.

The fitting of Eq. (1) to the experimental data is shown in Fig. 5 (see insets). The agreement of both theoretical and experimental curves for all samples in a large range of temperatures (40 K < T < 260 K) confirms that the transport in that region is governed by the variable range hopping process. Also, the fitting procedure of Eq. (1) provides $\alpha^{-1}=5$–40 Å which in turn is close to the accepted value of the $LaNiO_3$ mean free path (23–30 Å) [29,35] and confirms the localized character of the transport. This value was calculated by considering the uniformly distributed energy states, and it is reasonable for the spatial extension of the carrier wavefunction in our samples. The density of states $N(E_F)$ was considered as $1.1–4.7\times10^{23}$ eV^{-1} cm^{-3} [47,48]. Additionally, this length is smaller than the cross-section of the sample which is in agreement with the three-dimensional character of the samples. From these results, samples grown on the (1 0 0) $SrLaAlO_4$ substrate show no MIT as expected for bulk $LaNiO_3$. In fact, the observation of the VRH mechanism above shows that these samples are in the insulating phase of MIT and electronically behaves as a three-dimensional material.

Surprisingly, samples grown on (0 0 1) $SrLaAlO_4$ single crystal substrates show a distinct behavior, Fig. 7. Changes in the electrical behavior of the films, as a function of temperature as the thickness is varied is clearly evident in Fig. 7. The 50 nm thick sample still shows a localized behavior for transport which agrees with the VRH model (see inset) for $\alpha^{-1}=10$ Å. However, for LNO thin film with a thickness of 50 nm and growth on (0 0 1) $SrLaAlO_4$ single crystal substrate the behavior is insulating over the entire temperature range. Boris et al. [2] reported a similar result to superlattices composed of thick consecutive layers of $LaNiO_3$ and $LaAlO_3$ on (0 0 1) $SrLaAlO_4$ single crystal substrate growth by pulsed laser deposition. The breakpoint between conduction regimes is at 100 K and is evident in the 100 nm thick samples when the insulating behavior is replaced by a metallic behavior as expected in MIT. Above this limiting value, the conduction mechanism shows a metallic character; as the temperature and phonon excitation increase, the amount of scattering events experienced by the conduction electrons increase as well which results in greater (metal) resistance. Below 100 K, the resistivity data show a localized character which in turn has the very same origin as observed in samples grown on (1 0 0) substrates.

The Ioffe-Regel criterion for MIT takes place when $k_F\ell=1$ where k_F is the Fermi wavelength and ℓ is the mean free path [49]. This requirement is fulfilled by samples grown on (0 0 1) substrates: $k_F\ell\sim0.4$ (100 nm thick) and $k_F\ell\sim0.9$ (450 nm thick). The increase in the resistance for temperatures higher than 100 K can be understood by considering the electron-phonon scattering mechanism (at low disorder limits). This behavior agrees very well with the Bloch–Grüneisen theory for the dependence of the electrical resistance on the electron-acoustic phonon scattering mechanism. Thus, the resistance is described by [50,51].

$$\rho(T)=\rho_0+A\left(\frac{T}{\Theta_D}\right)^n\int_0^{\frac{\Theta_D}{T}}\frac{z^n e^z}{(e^z-1)^2}dz, \quad (2)$$

where A and R_0 are constants and n usually ranges from 3 to 5 when the electron–phonon interaction is mainly responsible for scattering events [38]; Θ_D is the Debye temperature. When the $T \geq \Theta_D$, all phonon modes are excited, and the resistivity increases linearly with increasing temperature. However, when $T \leq \Theta_D$, phonon scattering is mostly dominated by one-phonon normal processes where only small scattering vectors contribute [50]. The fitting of experimental data using Eq. (2) revealed $n=5$ and $\Theta_D=733$ K (100 nm sample) and 481 K (450 nm sample). As the temperature and phonon excitation increase, the amount of scattering events experienced by conduction electrons increase as well which results in greater resistance. From the literature [48,52,53], Θ_D=385–500 K. The observed Debye temperature is a definitive proof th at electron–phonon interaction and then a metallic phase are dominating the conduction mechanism in those samples. Importantly, the 100 nm thick sample has a high value of Θ_D due to the clear presence of two different coexisting conduction mechanisms. To confirm the metallic phase, a thicker sample (1000 nm) was fabricated; as expected, Θ_D=478 K (not shown here).

From resistivity data plotted in Fig. 6 (100 nm and 450 nm samples), the linear region observed in the resistivity can be used to estimate the electron–phonon coupling constant given by [41,54,55].

$$\lambda = \frac{\hbar\omega_P^2}{8\pi^2 k_B}\left[\frac{d\rho}{dT}\right], \tag{3}$$

where ω_P is the plasma frequency, and the other symbols have their usual meanings. The plasma frequency can be calculated from Drude formalism [56] which yields $\hbar\omega_P \sim 1.1$ eV and then $\lambda \sim 1.0$. This value is comparable with the typical value LNO ($\lambda=0.14$–0.8) [47,57], but it is higher than values observed in the literature because the linear region of resistivity chosen for the calculation is different in a transition region when the electron–phonon scattering changes from one-phonon processes to include all excited phonon modes. In fact, as the temperature range used for resistivity measurements is lower than Θ_D (the higher temperature used is close to Θ_D), the resistivity of the samples seems to be dominated by one-phonon processes ($\rho \sim T^5$). Thus, these higher λ values should be used carefully; they are not associated with a higher electron–phonon interaction (as would be expected from Jahn–Teller distortion [58]).

An in-depth investigation of experimental data provides other interesting features. The dependence of the observed conduction mechanisms on the sample thickness and crystallographic direction is part of a general picture where disorder plays a fundamental role. The literature verifies that the stoichiometric LNO is a charge transfer metal in which the metallic or insulating phases are determined by the interplay between band width, on-site Coulomb energy and the position of p bands (from non-metallic elements). In the metallic phase, bands are combined into a single band where the Fermi level falls [40]. However, when oxygen vacancies are present (non-stoichiometric material, i.e. highly oxygen deficient $LaNiO_{3-\delta}$, $\delta \geq 0.25$), an additional p band of the non-metallic element appears at an energy between the metallic d bands which leads to the insulator behavior. In our case, all the samples are considered stoichiometric in such a way that the position of the Fermi level is fixed for all of them (it was calculated to be $E_F=0.21$ eV from the density of electrons by considering one conduction electron from each Ni atom).

After these considerations, we believe that the observed MIT in our samples comes from a slightly different mechanism where the key parameter seems to be the disorder. Localized and nonlocalized states induced by disorder are separated by mobility edges generally delimited by band tails (see Fig. 8,

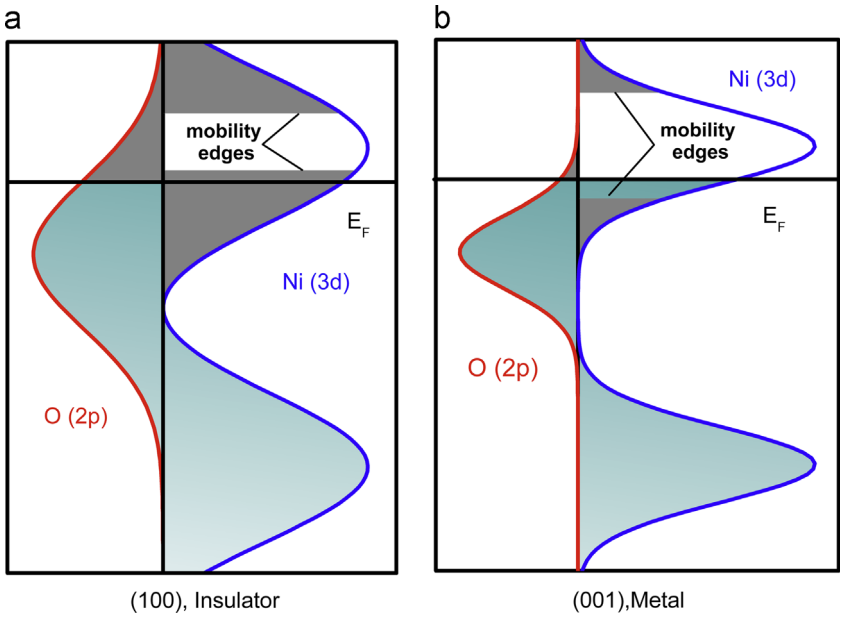

Fig. 8. Schematic density-of-states diagram showing the proposed mechanism of the electronic conduction switching process; (a) Insulator and (b) Metallic behavior. (For interpretation of the references to color in this figure legend, the reader is referred to the web version of this article.)

proposed mechanism). Considering that free charges in LNO contributing to the conduction come from the interplay between 3d (Ni) and 2p (O) bands, the mobility edge position is the critical criterion determining global conductivity. In addition, in the Fig. 8, blue and red lines refer to the contribution of nickel 3d and oxygen 2p states to the total density of states, respectively. The transition happens locally when the Fermi energy passes across the mobility edge. Band tails are mainly composed of localized states with low mobility due to disorder in these systems. When the Fermi energy is located inside the grey area (see Fig. 8a), samples will display an insulating-like behavior (for any thickness), in other words, the insulator state appears when the disorder is sufficiently large to spread the localized states in a broad range of energies and the Fermi level is located at these states. However, the metallic state is observed when the disorder is small and the Fermi level is located at the mobility edge, a metallic-like transport occurs (see Fig. 8b); consequently, the film conductivity increases. Thus the conductivity is drastically reduced because localized states do not contribute to conduction which leads to the observed insulating behavior. Since the position of the Fermi level is fixed for both samples, MIT is in fact the result of different disorder intensities. The observed changes on the degree of orientation for different samples provides a clue to what is happening: weaker textured samples imply a high level of disorder which leads to the characteristic electron localization of the insulating phase which is thermodynamically stable and is related only to the localized states in O (2p) Ni (3d) bands.

4. Conclusions

In this work, crystalline LNO thin films were obtained by chemical solution deposition method on both (1 0 0)- and (0 0 1)-oriented $SrLaAlO_4$ single crystal substrates. It was shown that the microstructure, structural and electric properties measurements is greatly dependent substrates crystallographic orientation and thin films thickness. The X-ray diffraction analysis indicated high degree preferential orientation along the (0 0 l) direction for LNO thin films on (0 0 1)-oriented $SrLaAlO_4$ substrate than on (1 0 0)-oriented $SrLaAlO_4$ substrates. The AFM images reveal that the LNO thin films growth onto both (1 0 0) and (0 0 1) $SrLaAlO_4$ single crystalline substrates exhibited homogenous grain distribuion, atomically smooth surface and pinhole-free. A general picture of the transport properties was constructed. In fact, the underlying mechanism discussed is based on the interplay of disorder, crystallographic orientation and thickness. We argue that the degree of orientation for different samples implies a high level of disorder; electron localization then occurs. MIT is a result of the competition between a mobility edge and the Fermi energy through the occupation of electron states which in turn is controlled by the disorder level induced by different growth surfaces. The present results further suggest that by choosing an appropriate thickness, substrate and crystallographic orientation, we can still achieve a $LaNiO_3$ thin film with metallic or insulating behavior.

Acknowledgments

This work was financially supported by the Brazilian agencies FAPESP, CNPq and CAPES. We thank CEPID/CMDMC/INCTMN. FAPESP process n°. 08/57150-6 and n°.11/20536-7.

References

[1] R.J. Zeches, M.D. Rossell, J.X. Zhang, A.J. Hatt, Q. He, C.-H. Yang, A. Kumar, C.H. Wang, A. Melville, C. Adamo, G. Sheng, Y.-H. Chu, J. F. Ihlefeld, R. Erni, C. Ederer, V. Gopalan, L.Q. Chen, D.G. Schlom, N. A. Spaldin, L.W. Martin, R. Ramesh, A strain-driven morphotropic phase boundary in $BiFeO_3$, Science 326 (2009) 977–980.

[2] A.V. Boris, Y. Matiks, E. Benckiser, A. Frano, P. Popovich, V. Hinkov, P. Wochner, M. Castro-Colin, E. Detemple, V.K. Malik, C. Bernhard, T. Prokscha, A. Suter, Z. Salman, E. Morenzoni, G. Cristiani, H.-U. Habermeier, B. Keimer, Dimensionality control of electronic phase transitions in nickel-oxide superlattices, Science 332 (2011) 937–940.

[3] H. German, S. Nicola, Shedding light on oxide interfaces, Science 332 (2011) 922–923.

[4] S. Valencia, A. Crassous, L. Bocher, V. Garcia, X. Moya, R.O. Cherifi, C. Deranlot, K. Bouzehouane, S. Fusil, A. Zobelli, A. Gloter, N. D. Mathur, A. Gaupp, R. Abrudan, F. Radu, A. Barthélémy, M. Bibes, Interface-induced room-temperature multiferroicity in $BaTiO_3$, Nature Mater 10 (2011) 753–758.

[5] R.G. Moore, Jiandi Zhang, V.B. Nascimento, R. Jin, Jiandong Guo, G. T. Wang, Z. Fang, D. Mandrus, E.W. Plummer, A surface-tailored, purely electronic, Mott metal-to-insulator transition, Science 318 (2007) 615–619.

[6] J.M. Rondinelli, N.M. Caffrey, S. Sanvito, N.A. Spaldin, Electronic properteis of bulk and thin film $SrRuO_3$: search for the metal-insulator transition, Physical Review B: Condensed Matter 78 (2008) 155107–155122.

[7] N. Gayathri, A.K. Raychaudhuri, X.Q. Xu, J.L. Peng, R.L. Greene, Magnetoresistance of the metallica perovskite oxide $LaNiO_{3-\delta}$, Journal of Physics: Condensed Matter 11 (1999) 2901.

[8] P. Lacorre, J.B. Torrance, J. Pannetier, A.I. Nazzal, P.W. Wang, T. C. Huang, Synthesis, crystal structure, and properties of metalliec $PrNiO_3$: comparison with metallic $NdNiO_3$ and semiconducting $SmNiO_3$, Journal of Solid State Chemistry 91 (1991) 225–237.

[9] H. Han, J. Zhong, S. Kotru, P. Padmini, X.Y. Song, R.K. Pandey, Improved ferroelectric property of $LaNiO_3/Pb(Zr_{0.2}Ti_{0.8})O_3/LaNiO_3$ capacitors prepared by chemical solution deposition on platinized silicon, Applied Physics Letters 88 (2006) 092902–092904.

[10] D. Bao, K. Ruan, T. Liang, Structure and electrical properties of Pb $(Zr_{0.25}Ti_{0.75})O_3$ thin films on $LaNiO_3$—coated thermally oxidized Si substrates, Journal of Sol–Gel Science and Technology 42 (2007) 353–356.

[11] R. Martinez, A. Kumar, R. Palai, R.S. Katiyar, J.F. Scott, Study of physical properties of integrated ferroelectric/ferromagnetic heterostructures, Journal of Applied Physics 107 (2010) 114107–114112.

[12] X. Yang, X. Wu, W. Ren, P. Shi, X. Yan, H. Lei, X. Yao, Effects of $LaNiO_3$ buffer layers on preferential orientation growth and properties of $PbTiO_3$ thin films,, Ceramics International 34 (2008) 1035–1038.

[13] T. Li, G. Wang, D. Remiens, X. Dong, Characteristics of highly (0 0 1) oriented (K, Na)NbO_3 films grown on $LaNiO_3$ bottom electrodes by RF magnetron sputtering,, Ceramics International 39 (2013) 1359–1363.

[14] L. Qiao, X. Bi, Effect of different buffer layers on the microstructure and dielectric properties of $BaTiO_3$ thin films grown on Si substrates, Journal of Alloys and Compounds 477 (2009) 560–564.

[15] F.M. Pontes, E.R. Leite, G.P. Mambrini, M.T. Escote, E. Longo E, J. A. Varela, Very large dielectric constant of highly oriented $Pb_{1-x}Ba_xTiO_3$ thin films prepared by chemical deposition, Applied Physics Letters 84 (2004) 248–250.

[16] R. Scherwitzl, S. Gariglio, M. Gabay, P. Zubko, M. Gibert, J. M. Triscone, Metal-insulator transition in ultrathin $LaNiO_3$ films, Physical Review Letters 106 (2011) 246403–246407.

[17] A.X. Gray, A. Janotti, J. Son, J.M. LeBeau, S. Ueda, Y. Yamashita, K. Kobayashi, A.M. Kaiser, R. Sutarto, H. Wadati, G.A. Sawatzky, C. G. Van de Walle, S. Stemmer, C.S. Fadley, Insulating state of ultrathin epitaxial $LaNiO_3$ thin films detected by hard X-ray photoemission, Physical Review B: Condensed Matter 84 (2011) 0751041 075110.

[18] J. Son, P. Moetakef, J.M. LeBeau, D. Ouellette, L. Balents, S.J. Allen, S. Stemmer, Low-dimensional Mott material: transport in ultrathin epitaxial $LaNiO_3$ films, Applied Physics Letters 96 (2010) 0621141–0621143.

[19] E. Detemple, Q.M. Ramasse, W. Sigle, G. Cristiani, H.-U. Habermeier, E. Benckiser, A.V. Boris, A. Frano, P. Wochner, M. Wu, B. Keimer, P. A. van Aken, Polarity-driven nickel oxide precipitation in $LaNiO_3$–$LaAlO_3$ superlattices, Applied Physics Letters 99 (2011) 2119031–2119033.

[20] H-Y. Lee, C.-H. Hsu, Y.-W. Hsieh, Y-H Chen, Y-C. Liang, T-B. Wu, L. J. Chou, Preparation of heteroepitaxial $LaNiO_3$ thin films on a $SrTiO_3$ substrate for growing an artificial superlattice with RF sputtering, Materials Chemistry and Physics 92 (2005) 585–590.

[21] X.T. Li, P.Y. Du, C.L. Mak, K.H. Wong, Epitaxial growth and dielectric properties of $Pb_{0.4}Sr_{0.6}TiO_3$ thin films on (0 0 *l*)-oriented metallic $Li_{0.3}Ni_{0.7}O_2$ coated MgO substrates, Applied Physics Letters 90 (2007) 2629061–2629063.

[22] C. Wang, M.H Kryder, Epitaxial growth of $LaNiO_3$ thin films on Si substrates using rf sputtering, Physica Scripta 78 (2008) 035601–035606.

[23] Z. El-Gohary, M. El-Nahass, H. Soliman, Y.L. El-Kady, Optical dispersion parameters with different orientation for $SrLaAlO_4$ single crystals, Journal of Materials Science and Technology 19 (2003) 77–80.

[24] G.H. Aydogdu, S.D. Ha, B. Viswanath, S. Ramanathan, Epitaxy, strain, and composition effects on metal-insulator transition characteristics of $SmNiO_3$ thin films, Journal of Applied Physics 109 (2011) 1241101–1241106.

[25] R.J. Ong, D.A. Payne, Processing effects for integrated PZT: residual stress, thickness, and dielectric properties, Journal of the American Ceramic Society 88 (2005) 2839–2847.

[26] D.R. McKenzie, M.M.M. Bilek, Thermodynamic theory for preferred orientation in materials prepared by energetic condensation, Thin Solid Films 382 (2001) 280–287.

[27] J Cao, J Wu, Strain effects in low-dimensional transition metal oxides, Materials Science and Engineering Reports 71 (2011) 35–52.

[28] L. Yang, G. Wang, C. Mao, Y. Zhang, R. Liang, C. Soyer, D. Rémiens, X. Dong, Orientation control of $LaNiO_3$ thin films by RF magnetron sputtering with different oxygen partial pressure, Journal of Crystal Growth 311 (2009) 4241–4246.

[29] C. Wang, B.L. Cheng, S.Y. Wang, H.B. Lu, Y.L. Zhou, Z.H. Chen, G. Z. Yang, Effects of oxygen pressure on lattice parameter, orientation, surface morphology and deposition rate of $(Ba_{0.02}Sr_{0.98})TiO_3$ thin films grown on MgO substrate by pulsed laser deposition, Thin Solid Films 485 (2005) 82–89.

[30] B. Ma, G.K.L. Goh, J.M., T.J. White, Growth kinetics and cracking of liquid-phase-deposited anatase films, Journal of the Electrochemical Society 154 (2007) D557–D561.

[31] T. Kubo, H. Nozoye, Surface structure of $SrTiO_3$(1 0 0), Surface Science 542 (2003) 177–191.

[32] X. Wang, S. Olafsson, P. SandstroÈm, U. Helmersson, Growth of $SrTiO_3$ thin films on $LaAlO_3$ (0 0 1) substrates; the infuence of growth temperature on composition, orientation, and surface morphology, Thin Solid Films 360 (2000) 181–186.

[33] J. Zhu, L. Zheng, Y. Zhang, X.H. Wei, W.B. Luo, Y.R. Li, Fabrication of epitaxial conductive $LaNiO_3$ films on different substrates by pulsed laser ablation, Materials Chemistry and Physics 100 (2006) 451–456.

[34] M. Radović, M. Salluzzo, Z. Ristić, R. Di Capua, N. Lampis, R. Vaglio, F.M. Granozio, In situ investigation of the early stage of TiO_2 epitaxy on (0 0 1) $SrTiO_3$, Journal of Chemical Physics 135 (2011) 034705–34712.

[35] D.G. Schlom, L-Q. Chen, C.-B. Eom, K.M. Rabe, S.K. Streiffer, J.-M. Triscone, Strain tuning of ferroelectric thin films, Annual Review of Materials Research 37 (2007) 589–626.

[36] H. Asaoka, Y. Machida, H. Yamamoto, K. Hojou, K. Saiki, A. Koma, Stress evolution during epitaxial growth of SrO films on hydrogen-terminated Si (1 1 1) surfaces, Solid State Communications 124 (2002) 239–242.

[37] A. Antonakos, E. Liarokapis, G.H. Aydogdu, H.U. Habermeier, Strain induced phase separation on $La_{0.5}Ca_{0.5}MnO_3$ thin films, Journal of Magnetism and Magnetic Materials 323 (2011) 620–630.

[38] M. Pervolaraki, I. Pasuk, G.E. Stan, J. Giapintzakis, Pulsed laser deposition of highly textured $La_5Ca_9Cu_{24}O_{41}$ films on $SrLaAlO_4$ (1 0 0) and $Gd_3Ga_5O_{12}$ (1 0 0) substrates, Applied Surface Science 258 (2012) 9475–9479.

[39] W. Noun, B. Berin, Y. Dumont, P.R. Dahoo, N. Keller, Correlation between electrical and ellipsometric properties on high-quality epitaxial thin films of the conductive oxide $LaNiO_3$ on STO (001), Journal of Applied Physics 102 (2007) 0637091–0637097.

[40] K. Tsubouchi, I. Ohkubo, H. Kumigashira, Y. Matsumoto, T. Ohnishi, M. Lippmaa, H. Koinuma, M. Oshima, Epitaxial growth and surface metallic nature of $LaNiO_3$ thin films, Applied Physics Letters 92 (2008) 2621091–2621093.

[41] G.P. Mambrini, E.R. Leite, M.T. Escote, A.J. Chiquito, E. Longo, J. A. Varela, R.F. Jardim, Structural, microstructural, and transport properties of highly oriented $LaNiO_3$ thin films deposited on $SrTiO_3$ (1 0 0) single crystal, Journal of Applied Physics 102 (2007) 0437081–0437086.

[42] M.S. Awan, A.S. Bhatti, S. Qing, C.K. Ong, Fabrication of LSS bottom electrode by PLD, Vacuum 85 (2010) 55–59.

[43] L. Qiao, X. Bi, Effect of substrate temperature on the microstructure and transport properties of highly (1 0 0)-oriented $LaNiO_{3-\delta}$ films by pure argon sputtering, Journal of Crystal Growth 310 (2008) 3653–3658.

[44] P.W. Anderson, Absence of diffusion in certain random lattices, Physical Review 109 (1958) 1492–1505.

[45] Yu.A. Pusep, A.J. Chiquito, S. Mergulhão, A.I. Toropov, Parallel conductivity of random GaAs/AlGaAs superlattices in regime of controlled vertical disorder, Journal of Applied Physics 92 (2002) 3830–3835.

[46] N.F. Mott, Metal Insulator Transitions, Taylor and Francis, London, 1990.

[47] L. Qiao, X. Bi, Nanostructure and performance of Pt–$LaNiO_3$ composite film for ferroelectric film devices, Acta Materialia 57 (2009) 4109–4114.

[48] K.P. Rajeev, G.V. Shivashankar, A.K. Raychaudhuri, Low-temperature electronic properties of a normal conducting perovskite oxide ($LaNiO_3$), Solid State Communications 79 (1991) 591–595.

[49] B.L. Al'tshuler, A.G. Aronov, Electron–Electron Interaction in Disordered Conductors, North Holland, Amsterdam, 1985.

[50] J.M. Ziman, Electrons and Phonons, Claredon Press, Oxford, 1960.

[51] A.J. Chiquito, A.J.C. Lanfredi, R.F.M. de Oliveira, L.P. Pozzi, E.R. Leite, Electron Dephasing and Weak Localization in Sn Doped In_2O_3 Nanowires Nanoletters, Nanoletters 7 (2007) 1439–1443.

[52] R.D. Sánchez, M.T. Causa, J. Sereni, M. Vallet-Regí, M.J. Sayagués, J. M. González-Calbet, Specific heat, magnetic susceptibility and electrical resistivity measurements on $LaNiO_3$, Journal of Alloys and Compounds 191 (1993) 287–289.

[53] C.E. Methfessel, G.R. Stewart, B.T. Matthias, C.K.N. Patel, Why is there no bulk specific heat anomaly at the superconducting transition temperature of $BaPb_{1-x}Bi_xO_3$?, Proceedings of the National academy of Sciences of the United States of America 77 (1980) 6307–6308

[54] M.T. Escote, V.B. Barbeta, R.F. Jardim, J. Campo, Metal–insulator transition in $Nd_{1-x}Eu_xNiO_3$ compounds, Journal of Physics: Condensed Matter 18 (2006) 6117–6132.

[55] M. Gurvitch, A.T. Fiory, Resistivity of $La_{1.825}Sr_{0.175}CuO_4$ and $YBa_2Cu_3O_7$ to 1100 K: absence of saturation and its implications, Physical Review Letters 59 (1987) 1337–1340.

[56] N.W. Ashcroft, N.D. Mermin, in: Solid State Physics, Holt, Rinehart and Winston, New York, 1976.

[57] S. Pal, B.K. Chaudhuri, S. Neeleshwar, Y.Y. Chen, H.D. Yang, Transport and magnetic properties of metallic $La_{1-x}Pb_xNiO_{3-\delta}$ ($0.0 \leqslant x \leqslant 0.1$), Journal of Applied Physics 97 (2005) 0437071–0437076.

[58] A.J. Millis, B.I. Shraiman, R. Muellar, Dynamic Jahn–Teller effect and colossal magnetoresistance in $La_{1-x}Sr_xMnO_3$, Physical Review Letters 77 (1996) 175–178.